Osmotic Pressure of Uncharged and Weakly Charged Oil/Water Microemulsion Droplets

H. Bagger-Jörgensen,*,† U. Olsson, and B. Jönsson

Physical Chemistry 1, Chemical Center, University of Lund, P.O. Box 124, S-221 00 Lund, Sweden

Received: April 2, 1997; In Final Form: May 30, 1997[⊗]

The osmotic pressure of uncharged and weakly charged spherical oil-in-water microemulsion droplets was measured as a function of the droplet volume fraction, ϕ, in the concentration range $0.06 \leq \phi \leq 0.44$. The data from the uncharged droplets were analyzed in terms of a hard-sphere repulsion in combination with a van der Waals attraction. The droplet size, as obtained from the analysis, shows a good agreement with previously published small-angle neutron and light scattering data. The droplets were made weakly charged by replacing a small fraction (0.01, 0.04, and 0.06) of the nonionic surfactant with ionic surfactant, retaining the droplet size. The introduction of long-range electrostatic interactions resulted in a strong increase of the osmotic pressure. From comparison with model calculations, solving the Poisson−Boltzmann equation in the cell model, it is concluded that essentially all the ionic surfactant adsorbs to the droplets for $\phi > 0.1$. At lower ϕ, however, the fraction of nonadsorbed ionic surfactant in the aqueous solvent becomes significant and increases with dilution. The degree of adsorption was also calculated within a molecular model, and a good agreement with the values obtained from the osmotic pressure data was found. When adding a large amount of salt to the charged droplets, the relevant osmotic pressure drops back to its original value for the uncharged case, demonstrating that the only influence of the ionic surfactant is the long-range electrostatic interaction.

1. Introduction

Osmotic pressure, directly related to the chemical potential of water, is a fundamental thermodynamic quantity in all colloidal systems, e.g., for controlling colloidal stability. Measurement of osmotic pressure is an inexpensive alternative to direct determination of molecular interaction, like direct force measurements, and is also directly applicable to most systems. In a colloidal solution with known microstructure, the osmotic pressure is related to the particle size and the interparticle interactions. Classically, the goal when measuring the osmotic pressure, Π, in colloidal chemistry was to obtain the molecular weight, e.g., for a polymer. Later, measurements of self-associated structures, like surfactant micelles, were also reported.[1−5] Together with the molecular weight, calculated from extrapolating Π/c to $c = 0$, where c is the concentration, the interparticle interaction may be obtained from the concentration dependence on Π, like the second virial coefficient or the osmotic compressibility. In our case, we have a former knowledge of the solution microstructure and are primarily interested in the interaggregate interaction, like the objectives of several osmotic stress studies.[6−8]

The system under investigation is composed of the nonionic surfactant pentaethylene glycol dodecyl ether ($C_{12}E_5$), water, and decane at a constant surfactant-to-oil weight ratio of 51.9/48.1. For oil-swollen, normal micelles, this corresponds to keeping the total interfacial area to enclosed volume ratio constant. A partial schematic phase diagram (omitting most multiphase regions) of the water-rich part (≥60 wt % water) is shown in Figure 1 (data taken from ref 9). The phase diagram is plotted as temperature versus the total volume fraction of surfactant and oil, ϕ. Referring to the phase diagram, a microemulsion phase (L_1) is stable within the temperature interval of approximately 25−32 °C. At lower temperatures, the microemulsion coexists with an essentially pure oil phase ($L_1 + O$). The L_1 phase terminates at about 32 °C. At slightly higher temperatures a lamellar liquid crystalline phase (L_α) is formed.

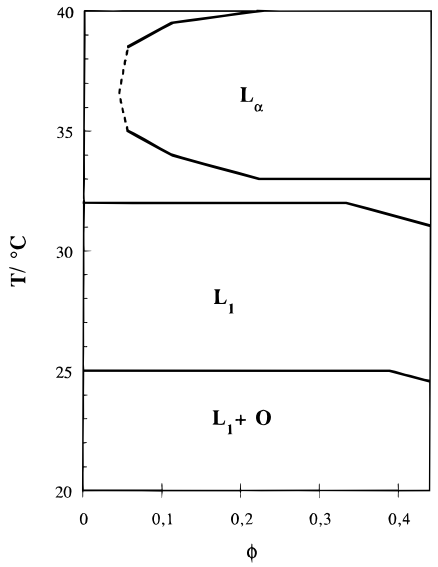

Figure 1. Partial phase diagram of the $C_{12}E_5$−H_2O−decane system (redrawn from ref 9) for a constant weight ratio, 51.9/48.1, of $C_{12}E_5$−decane. The phase diagram is drawn as temperature versus the total volume fraction of surfactant and oil, $\phi = \phi_s + \phi_o$. In this temperature and concentration interval, only two single-phase regions are detected: the microemulsion phase (L_1) and the lamellar liquid crystalline phase (L_α). $L_1 + O$ is a two-phase area where the microemulsion is in equilibrium with excess oil. At the lower phase boundary (emulsification failure), the microemulsion consists of spherical oil-swollen micelles with low polydispersity.

The microstructure of the microemulsion phase depends on the temperature and the surfactant plus oil concentration. The lower phase boundary is, however, of particular significance. On this boundary, which corresponds to the saturation limit of oil solubilization, also denoted emulsification failure, the microstructure corresponds to spherical oil droplets, which here have a hydrocarbon radius of 75 Å and are of low polydispersity

† Present address: Astra Draco AB, P.O. Box 34, S-221 00 Lund, Sweden.

⊗ Abstract published in *Advance ACS Abstracts,* July 15, 1997.

S1089-5647(97)01156-5 CCC: $14.00

(≈16%).[10] Hence, this phase boundary is an ideal location for measuring the osmotic pressure versus the droplet volume fraction since both the microstructure and the phase boundary temperature are independent of ϕ. Increasing the temperature away from this boundary results in a slight growth of the micelles into nonspherical shapes and, for higher ϕ, the formation of a bicontinuous structure.[11,12] Hence, it is essential that Π really is measured along the lower phase boundary, since otherwise the droplets may be nonspherical. The polar/apolar interface, separating the pentaethylene oxide from the hydrocarbon chain of the surfactant monolayer, has an essentially invariant area per molecule.[13−15] The droplets can be pictured as hydrocarbon spheres, containing oil and the alkyl chains of the surfactant, coated with a layer of "end-grafted" pentaethylene oxide chains. The alkyl chains make up approximately half of the surfactant volume. The hydrocarbon volume fraction, ϕ_{hc}, is thus given by $\phi_{hc} = \phi_o + 0.5\ \phi_s$, where ϕ_o and ϕ_s are the volume fraction of oil and surfactant, respectively. Since the surfactant-to-oil volume ratio $\phi_s/\phi_o = 45/55$, ϕ_{hc} is related to the total volume fraction ϕ by $\phi_{hc} = 0.775\phi$. Previous studies on this system close to the lower phase boundary have shown to be consistent with the micelles interacting as hard spheres.[9,16]

There are several ways of measuring the osmotic pressure.[17] Direct membrane osmometry[18] is the most direct way, whereas the osmotic stress technique[17] works in a more indirect way. Other alternatives are the isopiestic method[19] and measurement of the vapor pressure of water.[20,21] All the above methods have their own advantages and disadvantages, and the system under study is important when selecting the appropriate method. In our case, the pressures to be measured are low, and hence the two former methods are preferred due to higher sensitivity. The osmotic stress technique is less applicable to these systems since the equilibration time is normally long, and hence surfactant monomers may diffuse through the membrane on this time scale. We have therefore chosen membrane osmometry as our experimental tool. Several membrane osmometers are described in the literature,[2,22,23] from quite simple to more sophisticated architecture. In our laboratory we have constructed an osmometer that we think is optimal for our system. Despite its simplicity, it has a wide pressure range, 0.1−100 kPa, with high accuracy and reproducibility.

In this study we have measured the osmotic pressure along the emulsification failure boundary, where the oil-swollen micelles are spherical. We have also investigated the effect on the pressure on adding ionic surfactant to the system. The addition of ionic surfactant (SDS) is analyzed by solving the Poisson−Boltzmann equation within the cell model. The degree of adsorption of SDS to the nonionic surfactant film is obtained by fitting the experimental osmotic pressure to the PB model. A theoretical treatment of the SDS partitioning, based on the calculation of the chemical potential of the ionic surfactant in two regions, the micellar surfactant film and the aqueous region, is also presented.

2. Experimental Section

2.1. Materials. The nonionic surfactant pentaethylene glycol dodecyl ether ($C_{12}E_5$) was obtained from Nikko Ltd. Tokyo. Decane (99%) and sodium chloride (NaCl) were from Sigma, and SDS was from BDH Laboratory Supplies, Poole, Dorset (England). The water was of Millipore quality. The SDS was recrystallized three times in methanol. All other chemicals were used as received.

The volume fractions for the samples were calculated using the following densities (g/cm^3): 0.967 ($C_{12}E_5$), 0.998 (H_2O), 0.73 (decane). The effect of the added ionic surfactant on the surfactant density was neglected.

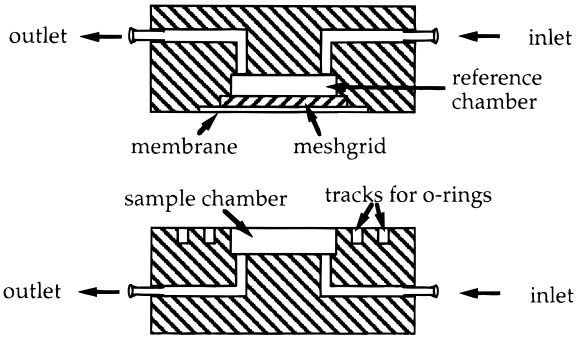

Figure 2. Side view of the two half-cells that make up the osmometer cell. The lower half-cell contains the sample chamber, while the upper half-cell contains the reference chamber. When the cell is mounted, the only connection between the two chambers is across the membrane. For further details, see text.

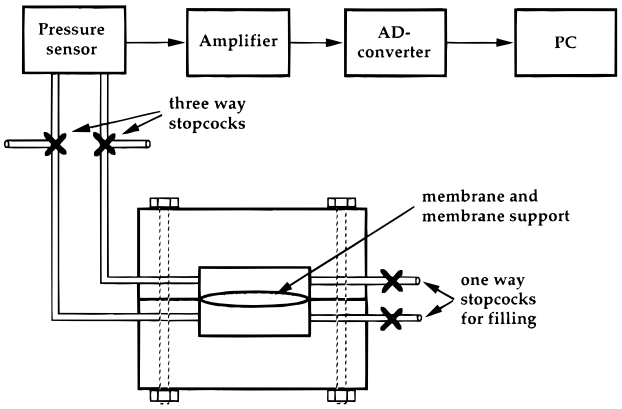

Figure 3. Schematic illustration of the complete osmometer. The difference between the hydrostatic pressures in the reference and sample chamber, mediated by thin hoses, is measured by a differential pressure sensor outside the osmometer cell. The pressure output as a function of time is registered by a computer.

2.2. The Osmometer. The construction of the osmometer cell is illustrated in Figure 2, and the overall construction of the full osmometer system is illustrated in Figure 3.

Osmometer Cell. The osmometer cell (Figure 2) consists of two parts, the upper and the lower half-cell. The half-cells are made from blocks of Plexiglas, into which cylindrical cavities for two compartments, the sample and reference chamber, have been milled. Note that the half-cells are not identical. Around the sample chamber, which is normally contained in the lower half-cell, are two concentrically milled tracks for two rubber "O"-rings. The unit containing the reference chamber, normally the upper half-cell, has two extra excavations for the membrane (0.2 mm deep) and for the membrane support (a mesh grid of stainless steel 1.0 mm thick). Drilled holes (diameter 3 mm) in both units serve as inlet and outlet to the chambers. Small brass nipples are screwed onto the outside of the cells, thus allowing further connections. The total dimension of the osmometer cell is 6 × 6 × 5 cm.

Full Osmometer. The full osmometer system is shown in Figure 3. The two half-cells are, after positioning the membrane support (mesh grid) and membrane, tightly screwed together with four screws. With the two "O"-rings present, the only connection between the sample and reference chamber is across the membrane. At the inlet of the osmometer cell, two one-way stopcocks are mounted to allow filling. On the outlet, two PVC hoses are connected to the outlet nipples. On the other end the hoses are connected to three-way stopcocks. From the stopcocks there are further hose connections to the pressure sensor. The pressure sensor we have used is of the silicon

piezoresistive type manufactured by Motorola. The sensor directly measures the differential pressure between the two pressure ports. The instrument is equipped with two different sensors, with maximum differential pressures of 10 and 100 kPa. The sensors are temperature compensated and are thus practically temperature insensitive up to ≈80 °C. They also have a good linearity and low-pressure hysteresis in the full pressure range. The analog output signal from the pressure sensor (0−25 mV) is first amplified 200 times (to 0−5 V) and then converted to a digital signal. The digitalized voltage signal is finally registered by a PC, transformed to a pressure output, and viewable on the screen as a function of time.

Principles of Operation, Calibration, and Performance. The 10 kPa pressure sensor was calibrated against a water column of varying height (0−1 m), since the hydrostatic pressure of 1 m water almost exactly equals 10 kPa. The linearity was also confirmed. The 100 kPa sensor was calibrated at low pressures against the same water column and at high pressures against Dextran solutions of known osmotic pressure.[17,24]

Before measurement, the hose between the three-way stopcock and the pressure sensor was partially filled with water. A small volume of air was left since this empirically was found to give a more stable pressure output with respect to time. The sample and reference (water) were filled into the respective chamber by opening the stopcocks and injecting the solution with a syringe. The CMC for $C_{12}E_5$ is very low (≈10^{-5} M),[25] and hence the monomeric contribution to Π is negligible (<0.025 kPa). Since the osmometer cell is fully transparent, air bubbles inside the chambers are easily detected and also easily removed by tilting the osmometer cell while filling. Typical volumes needed are ≈2 mL. After filling, the one-way stopcocks were closed and the three-way stopcocks were turned to connect the pressure sensor with the osmometer cell. Due to the small volume of air in the hose, a very small volume of water will pass through the membrane before equilibrium is reached. However, since the air volume is much smaller than the sample volume, this dilution effect is negligible in all cases. After filling, the osmometer cell is placed in a water bath (also transparent) for accurate temperature control. To reduce the measuring time and to ensure a homogeneous sample solution, a small magnet may be placed in the sample chamber, thus making magnetic stirring possible. The sample cell is rinsed by flushing with a large amount of water.

The membrane used in the osmometer experiments is denoted C10 and manufactured by Hoechst Ag, Frankfurt, Germany. The membrane is made of regenerated cellulose with a nominal molecular weight cutoff of 10 kDa. This membrane is non-penetrable for the oil-swollen micelles, while the water and the surfactant and oil monomers may pass through. However, the monomer concentration is very low and has a negligible effect on the osmotic pressure.

The performance of the osmometer was tested with Dextran (number-average molecular weight 110 kDa, Fluka), since the osmotic pressure for this polymer as a function of concentration has been reported by several authors.[17,24] Our values agreed nicely with the published values. The pressure as a function of time is shown in Figure 4 for a sample containing 30 wt % oil-swollen micelles. The pressure reaches a plateau value after about 40 min, after which it is constant for several hours. For longer times (days) a small decay of the pressure is noted, indicating that there is a small leakage between the two half-cells. However, this decay is negligible due to the fast equilibration time (less than an hour) compared to the time needed to see any decay in pressure.

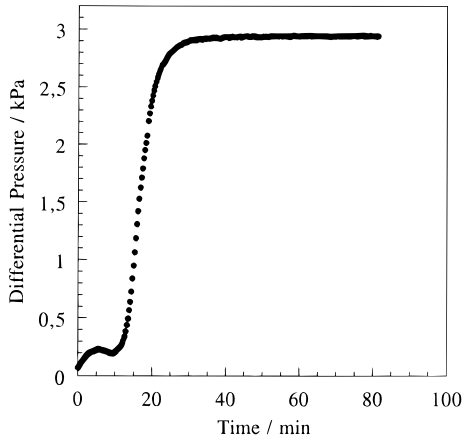

Figure 4. A typical differential pressure versus time measurement by the osmometer. The sample consists of 30 wt % of oil-swollen micelles, corresponding to $\phi = 0.34$. When the sample is loaded at $t = 0$, the differential pressure is close to zero. With time water flows into the sample chamber, causing the pressure to increase in the sample chamber and decrease in the reference chamber. At equilibrium there is no net water flow and the differential pressure is constant, equal to the osmotic pressure in the sample.

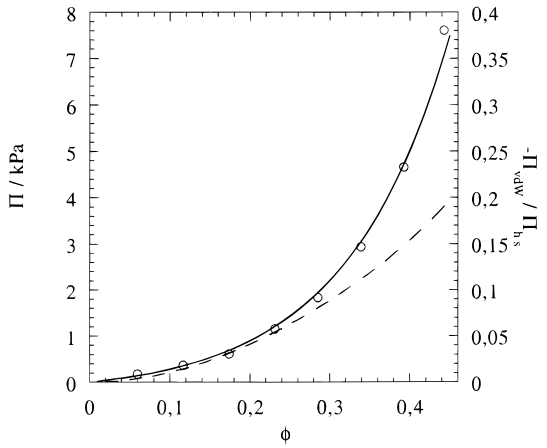

Figure 5. Measured osmotic pressure, Π, versus volume fraction, ϕ, at the lower phase boundary in the pure microemulsion system (○). The line represents a fit of the total pressure, $\Pi_{HS} + \Pi_{vdW}$, calculated according to eqs 1 and 3, to the measured pressure. The fit yields a droplet hydrocarbon radius $R_{hc} = 75$ Å and $\alpha = 1.07$, corresponding to a hard-sphere radius $R_{HS} = 84$ Å. The dashed line is the calculated ratio $-\Pi_{vdW}/\Pi_{HS}$ (right-hand scale). As seen from the figure, the van der Waals contribution is, except at very low concentrations, not negligible.

3. Results and Discussion

3.1. The Pure Surfactant−Water−Oil System. 3.1.1. The L_1 Phase. The osmotic pressure was measured in the microemulsion system (Figure 1) along the lower phase boundary ($L_1 + O \rightarrow L_1$) at 25.5 °C , where the micelles are spherical in the full concentration range ($0 < \phi < 0.45$). The result is shown in Figure 5, drawn as osmotic pressure, Π, versus volume fraction, ϕ. There are two major contributions to the osmotic pressure: (i) the repulsive hard-sphere interaction, lowering the chemical potential of water and thus giving a positive contribution to Π, and (ii) the attractive van der Waals interaction, raising the chemical potential of water and thus yielding a negative contribution to Π. A good description of a hard-sphere dispersion is given by the Carnahan−Starling equation of state[26]

$$\Pi_{HS} = k_B T n \left(\frac{1 + \phi_{HS} + \phi_{HS}^2 - \phi_{HS}^3}{(1 - \phi_{HS})^3} \right) \qquad (1)$$

where ϕ_{HS} is the hard-sphere volume fraction and n is the number density of spheres. The latter is given by

$$n = \frac{\phi_{hc}}{V_{hc}} = \frac{3\phi_{hc}}{4\pi R_{hc}^3} \quad (2)$$

where $\phi_{hc} = 0.775\phi$ is the hydrocarbon volume fraction and R_{hc} is the hydrocarbon radius of the droplet. The hard-sphere volume fraction is not necessarily equal to ϕ. Water is a good solvent (better than a θ-solvent) for ethylene oxide at this temperature,[27] and the EO chains are extended from the surface.[28] The hard-sphere volume fraction is thus considered to be proportional to ϕ with a proportionality constant α, i.e., $\phi_{HS} = \alpha\phi$.

The van der Waals contribution to the osmotic pressure is not straightforward to evaluate. In our analysis we will consider the interaction to be nonretarded at all compositions. This is strictly only true for separations below about 50 Å[29] and hence not directly applicable to the dilute samples. On the other hand, the vdW interaction is only important at higher concentrations, where also the interdroplet distance is below 50 Å. A further problem arises since we are dealing with a so-called triple-film problem (hydrocarbon−ethylene oxide−water). However, the Hamaker constant for poly(ethylene oxide)−water[30] is close to the value for hydrocarbon−water[31] (6×10^{-21} J), and hence we consider this value to be a good approximation for the whole particle. The van der Waals interaction between two spherical particles in the nonretarded case is known.[31] Depositing the spheres onto a lattice, summing up the nearest-neighbor interactions, and evaluating the partial derivative $\mu_w^{vdW} = (\partial G^{vdW}/\partial n_w)|n_p$, gives the van der Waals contribution to the osmotic pressure[32]

$$\Pi_{vdW} = -\frac{\mu_w^{vdW}}{v_w} = -k_B T n \frac{zH_{eff}}{36k_B T}\left(\frac{\phi^2}{(\phi_{cp} - \phi_{cp}^{1/3}\phi^{2/3})^2}\right) \quad (3)$$

where n again is the number density of spheres. H_{eff} is the effective Hamaker constant, chosen as the value of hydrocarbon−water (6×10^{-21} J), z is the coordination number in the lattice, and ϕ_{cp} is the volume fraction where close packing occurs. Here we have assumed a hexagonal lattice for which $z = 12$ and $\phi_{cp} = 0.74$.

The total osmotic pressure, $\Pi_{tot} = \Pi_{HS} + \Pi_{vdW}$, may now be fitted to the experimental osmotic data, using R_{hc} and α as fitting parameters. The result is presented in Figure 5 as a solid line, with the fitted parameters $R_{hc} = 75$ Å and $\alpha = 1.07$, corresponding to a hard-sphere radius $R_{HS} = 84$ Å. The dashed line in the figure (right-hand scale) shows the ratio of the two contributions, $-\Pi_{vdW}/\Pi_{HS}$. It is clearly seen that the van der Waals contribution is in this case, except at low ϕ, *not* negligible. The droplet (hydrocarbon) radius is in excellent agreement with previous studies,[9−11,15,33] whereas the constant α is slightly lower compared to a recent dynamic light scattering study (neglecting van der Waals interaction), where a value $\alpha = 1.14$ was observed.[9] This corresponds to a difference in hard-sphere radius of 2 Å.

The L_α Phase. The pressure in the lamellar phase formed around 38 °C was found to be more than an order of magnitude smaller than in the micellar phase and could therefore not be measured accurately. Preliminary experiments gave $\Pi \approx 0.4$ kPa for $\phi = 0.44$. That a low pressure is expected can be shown by estimating the positive and negative contributions to the pressure. Nonionic lamellar phases are stabilized by the (weak) undulation force.[34] Treating for simplicity the oil-swollen bilayer as a surface with a bending rigidity modulus κ, the contribution to the osmotic pressure for undulating bilayers is[35,36]

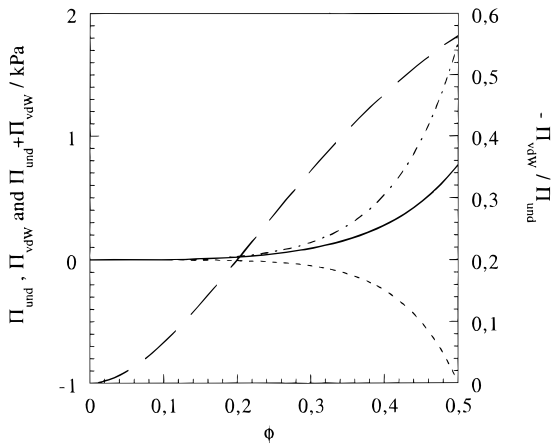

Figure 6. Undulation pressure, Π_{und} (dash-dot), calculated according to eq 4, the van der Waals pressure, Π_{vdW} (short dash), given by eq 6, and the total pressure, $\Pi_{und} + \Pi_{vdW}$ (solid), calculated for a bilayer bending modulus $\kappa = 4k_BT$, bilayer thickness $\delta = 64$ Å, and effective Hamaker constant $H_{eff} = 6 \times 10^{-21}$ J. The ratio Π_{vdW}/Π_{und} (long dash) is also shown in the right-hand scale. As seen from the figure, the van der Waals contribution reduces the total pressure substantially.

$$\Pi_{und} = \frac{3\pi^2}{64}\frac{(k_B T)^2}{\kappa}\frac{1}{\delta^3}\left(\frac{\phi}{1-\phi}\right)^3 \quad (4)$$

where δ is the bilayer thickness.

The van der Waals energy for an infinite array of water and hydrocarbon sheets can be written as[31]

$$G_{vdW} = -A\frac{H_{eff}}{12\pi\delta^2}\left\{\frac{1}{2} + \sum_{j=1}^{\infty}\frac{\phi^4}{j^4}\frac{3-(\phi^2/j^2)}{[1-(\phi^2/j^2)]^2}\right\} = -A\frac{f(\phi)}{\delta^2} \quad (5)$$

where A is the bilayer area, H_{eff} is the effective Hamaker constant, and δ is the bilayer thickness. The infinite series in the above equation is rapidly converging, and only a few terms are needed in the summation. The contribution to the osmotic pressure becomes[37]

$$\Pi_{vdW} = -\frac{2\phi^2}{\delta^3}\frac{\partial}{\partial\phi}f(\phi) \quad (6)$$

The total pressure, $\Pi_{und} + \Pi_{vdW}$, depends on the values of the bilayer bending modulus κ, the effective Hamaker constant H_{eff}, and the bilayer thickness, δ. As discussed in the previous section, $H_{eff} = 6 \times 10^{-21}$ J seems to be a reasonable value. From SAXS measurements, δ was found to be 64 Å.[13] The magnitude of κ can be estimated from a recent study of the same system, where $2\kappa + \bar{\kappa} = (3 \pm 0.5)k_BT$ was obtained in the micellar phase.[15] Here, κ is the monolayer bending modulus and $\bar{\kappa}$ is the saddle splay modulus. Since the bilayer bending modulus is twice the monolayer value and is expected to be negative and of smaller magnitude than κ,[38] a bilayer bending modulus of $4k_BT$ is reasonable in our case. Π_{und}, Π_{vdW}, and $\Pi_{und} + \Pi_{vdW}$ are plotted versus ϕ in Figure 6 with the above values of κ, H_{eff}, and δ. As seen from the figure, the contribution from the (attractive) van der Waals force is of comparable magnitude as that from the undulation force. The net stabilizing force, adding the repulsive undulation force with the attractive van der Waals force, is hence substantially smaller than if the van der Waals term is neglected. Thus, the calculation confirms that, in the study of stabilizing forces in

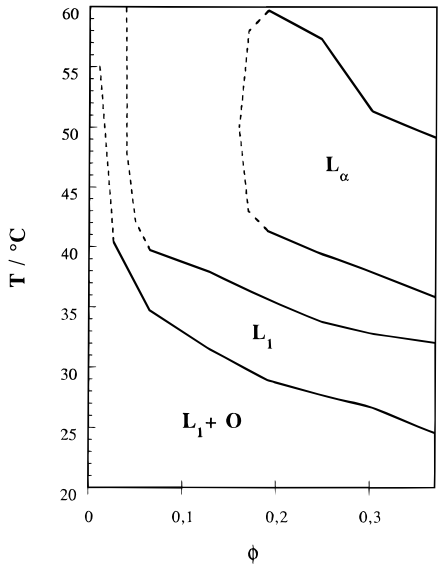

Figure 7. Nonionic surfactant film may be slightly charged by replacing $C_{12}E_5$ with the anionic surfactant SDS. The main features of the phase diagram are maintained. However, the phase boundaries are strongly concentration dependent, and the extent of the different phases is changed. As an example, we show what influence an exchange of 4 mol % of $C_{12}E_5$ by SDS ($\beta = 0.04$) has on the phase behavior (redrawn from ref 15). The notation is the same as in Figure 1. The full phase diagrams for all degrees of SDS modification can be found in refs 15 and 39.

sterically stabilized lamellar phases, the van der Waals contribution *cannot* be neglected.

3.2. Electrostatic Interactions. The nonionic surfactant film can be made weakly charged by adding small amounts of ionic surfactant.[15] Here, as in ref 15, this was done by replacing a certain amount of the nonionic $C_{12}E_5$ by the anionic surfactant sodium dodecyl sulfate (SDS). The SDS content is expressed as the mole fraction of SDS in the surfactant mixture, $\beta = n(\text{SDS})/n(C_{12}E_5 + \text{SDS})$. The phase behavior of the three systems $\beta = 0.01$, $\beta = 0.04$, and $\beta = 0.06$ has been studied previously.[15,39] The partial phase diagram for the $\beta = 0.04$ is schematically illustrated in Figure 7, redrawn from ref 15. Qualitatively the same phase behavior as for the uncharged system is found, although with temperature shifts in the phase boundaries. Replacing water with brine (0.1 M NaCl), and thereby screening the long-range electrostatic interaction, the phase diagram becomes almost identical to the pure, uncharged system.[15] Hence, the change in phase behavior upon adding SDS is of pure electrostatic origin. Although SDS in aqueous solution dissociates into sodium ions and dodecyl sulfate, we will refer to the surfactant as SDS despite the fact that the sodium ions are dissociated.

3.2.1. The L_1 Phase + SDS. The aim of this section is to study the interactions of the weakly charged droplets and to determine the partitioning of added ionic surfactant. We begin by considering the L_1 phase. Since the two surfactants, $C_{12}E_5$ and SDS, have the same hydrocarbon chain length and the nonionic surfactant is in great excess, the radius of the spherical micelle at the lower phase boundary is not significantly changed on addition of SDS. The measured osmotic pressure along the lower phase boundary versus ϕ for $\beta = 0.01$, $\beta = 0.04$, and $\beta = 0.06$ is presented in Figure 8. As seen from the figure, the pressure increases dramatically on addition of SDS.

The osmotic pressure in the charged system contains three components: the electrostatic interaction, Π_{el}, the contribution from aggregate mixing, Π_{mix}, and the van der Waals contribution, Π_{vdW}. The electrostatic interaction is the dominating

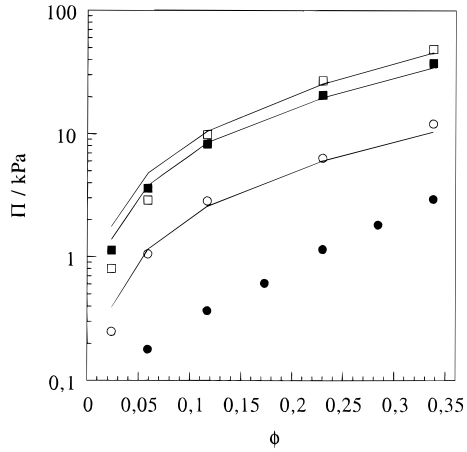

Figure 8. Osmotic pressure versus volume fraction, measured along the lower phase boundary, for different degrees of SDS doping: (○) $\beta = 0.01$, (■) $\beta = 0.04$, (□) $\beta = 0.06$. For comparison, Π in the $\beta = 0$ system (the pure microemulsion) is also shown (●). The lines are the calculated osmotic pressures, assuming full adsorption ($\rho = 1$) of SDS into the micellar surfactant film.

contribution (no excess electrolyte is present). The mixing entropy is difficult to quantify. The strong electrostatic repulsion makes the micelles to some extent ordered, resulting in a lower entropy of mixing than for hard spheres, i.e., $\Pi_{mix} < \Pi_{HS}$. Since we cannot directly quantify this reduction, and as we believe Π_{mix} to be much smaller than Π_{el}, we omit this term. Further, the van der Waals contribution, Π_{vdW}, is negligible compared to Π_{el}. Hence, we consider the only relevant contribution to the osmotic pressure to be the electrostatic interaction, i.e., $\Pi = \Pi_{el} + \Pi_{mix} + \Pi_{vdW} \approx \Pi_{el}$. The electrostatic contribution to the chemical potential of water was analyzed in the cell model,[40] where the total system is divided into identical, spherical cells. Each cell consists of a spherical micelle in the centre, surrounded by an aqueous solution. The cell radius, R_{cell}, is determined from the volume fraction of micelles, ϕ, by $\phi = R_{mic}^3/R_{cell}^3$. The Poisson−Boltzmann equation is then numerically solved for one cell.

The calculated osmotic pressure, assuming that all ionic surfactant is located in the micellar surfactant film, is shown as lines in Figure 8. As seen from the figure, the calculated pressure agrees almost perfectly with the experimental at $\phi \geq 0.12$, whereas the calculation overestimates the pressure at low ϕ. This indicates that only a fraction of the SDS molecules, ρ, defined as the ratio of the number of adsorbed SDS and the total number of SDS molecules, i.e., $\rho = n_{SDS}^{bound}/n_{SDS}^{tot}$, is adsorbed into the micellar surfactant film. Hence, we consider the equilibrium SDS(aqueous region) ↔ SDS(micelle), with the equilibrium presumably strongly shifted to the right.[15,41] The SDS in the water region is considered as monovalent salt. ρ may be calculated by considering the deviation of the experimental and calculated pressures drawn in Figure 8. The result is presented in Figure 9.

3.2.2. Theoretical Analysis. The aim of this section is to investigate the partitioning of SDS between the micellar surfactant film and the aqueous region on a theoretical basis. The nonionic, oil-swollen micelles are modeled as monodisperse spheres consisting of two parts: the hydrocarbon core, containing decane and the hydrophobic tails of the surfactant, and the micellar palisade layer, containing the polar headgroups of the surfactant and some water. The micelles exist within an aqueous region. Adsorption of SDS takes place by dissolving the dodecyl chain in the hydrocarbon core of the micelle. As previously discussed, the micellar size is considered as constant at the lower phase boundary upon replacement of $C_{12}E_5$ by SDS

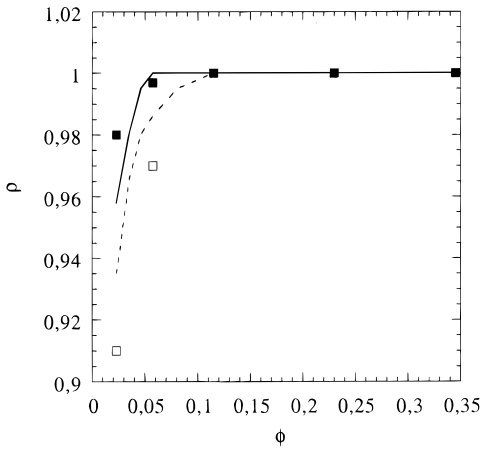

Figure 9. Fraction of adsorbed ionic surfactant into the micelles, ρ, versus ϕ. The symbols are values extracted from experiments: (■)) $\beta = 0.04$, (○) $\beta = 0.06$. The lines corresponding to $\beta = 0.04$ (solid) and $\beta = 0.06$ (dash) are from the theoretical treatment, calculated according to eqs 7 and 8.

(although the phase boundary temperatures are shifted, see Figure 7). To facilitate calculations, the cell model is used (see previous section). The electrostatic contribution to the chemical potential is calculated from the Poisson−Boltzmann equation. In the PB calculations, the charge is located at the interface between the hydrocarbon core and the palisade layer. Two expressions for the chemical potential of SDS, in the aqueous region, $\mu^{\text{tot}}_{\text{SDS,mon}}$, and in the micellar palisade layer, $\mu^{\text{tot}}_{\text{SDS,mic}}$, are considered.

For SDS in the palisade layer, the total chemical potential of SDS consists of three contributions: a mixing entropy term between $C_{12}E_5$ and SDS within the micelle, $\mu^{\text{mix}}_{\text{SDS,mic}}$, an electrostatic energy term, $\mu^{\text{el}}_{\text{SDS,mic}}$, and finally a standard chemical potential of SDS in the micellar palisade layer, $\mu^{\circ}_{\text{SDS,mic}}$, i.e.

$$\mu^{\text{tot}}_{\text{SDS,mic}} = \mu^{\text{mix}}_{\text{SDS,mic}} + \mu^{\text{el}}_{\text{SDS,mic}} + \mu^{\circ}_{\text{SDS,mic}} \tag{7}$$

For monomeric SDS in the aqueous region, two contributions make up the chemical potential: an electrostatic term, $\mu^{\text{el}}_{\text{SDS,mon}}$, and a standard chemical potential of SDS in the aqueous region, $\mu^{\circ}_{\text{SDS,w}}$, i.e.

$$\mu^{\text{tot}}_{\text{SDS,mon}} = \mu^{\text{el}}_{\text{SDS,mon}} + \mu^{\circ}_{\text{SDS,w}} \tag{8}$$

The expressions for the different contributions to the chemical potential of SDS are given below. For a more detailed description of the method, see ref 37.

Electrostatic Free Energy. The contribution to the chemical potential of SDS in the aqueous region becomes

$$\mu^{\text{el}}_{\text{SDS,mon}} = k_{\text{B}}T \ln(c_{\text{s0}}/c_0) \tag{9}$$

where c_{s0} is the SDS concentration at the cell border and c_0 is the concentration of water. The electrostatic contribution to the chemical potential of a SDS molecule in the palisade layer of the micelle, $\mu^{\text{el}}_{\text{SDS,mic}}$, is given by

$$\mu^{\text{el}}_{\text{SDS,mic}} = -e\Psi - \frac{V_{\text{j}}}{V_{\text{mic}}}\left\{E_{\text{el}} + k_{\text{B}}T\sum_i (n_i^{\text{w}} - V_{\text{hc}}N_{\text{A}}c_{i0}) + \frac{2E_{\text{el}}R_{\text{hc}}}{3(R - R_{\text{hc}})}\right\} \tag{10}$$

where e is the unit charge, Ψ is the electrostatic potential at the hydrocarbon−ethylene oxide/water interface, V_{SDS} is the hydrocarbon volume of SDS, V_{mic} is the total micellar volume, V_{hc} is the micellar hydrocarbon volume, n_i^{w} is the number of ions in the aqueous part of one cell, N_{A} is Avogadro's number, E_{el} is the electrostatic energy in one cell, and R is the total radius of the micelle. All quantities, except the volumes and the radii, are calculated from the PB equation.

Entropy of Mixing within a Micelle. The mixing of SDS and $C_{12}E_5$ gives a significant contribution to the surfactant chemical potential, which we approximate as ideal mixing

$$\mu^{\text{mix}}_{\text{SDS,mic}} = k_{\text{B}}T \ln X_{\text{SDS}} \tag{11}$$

Here, X_{SDS} is the mole fraction of SDS in the palisade layer.

Difference in Standard Chemical Potential. There is a large difference in standard chemical potential of SDS in the aqueous region and in the palisade layer, $\mu^{\circ}_{\text{SDS,w}}$ and $\mu^{\circ}_{\text{SDS,mic}}$, respectively. The major contribution to this difference is due to the difference in hydrocarbon/water contact, the "hydrophobic interaction". Other minor contributions are a difference in chain entropy and solvation of the headgroups, which are difficult to quantify. We have therefore, as has been done before,[42] calculated $\Delta\mu^{\circ}_{\text{SDS}}$ ($= \mu^{\circ}_{\text{SDS,w}} - \mu^{\circ}_{\text{SDS,mic}}$) from the experimental cmc value in the pure surfactant−water system (8.3 mM).[43] Micelle formation removes most of the hydrocarbon/water contact. There is, however, a residual interfacial energy at the micellar surface, which gives a contribution to the chemical potential of SDS in the micelle

$$\mu^{\text{int}}_{\text{SDS,mic}} = \gamma a_{\text{SDS}} \tag{12}$$

where γ is a constant that for several systems has been found to be close to 18 mJ/m^2,[44] and a_{SDS} is the surface area of a SDS molecule, which we assume to be the same as for $C_{12}E_5$, i.e., 48 Å^2. In a spherical SDS micelle near cmc, $a_{\text{SDS}} \approx 75$ Å^2.[45] Taking into account the difference in area per molecule in the two aggregates, the SDS micelle and the microemulsion droplet, we then obtain $\Delta\mu^{\circ}_{\text{SDS}} = 14.5\ k_{\text{B}}T$. If the interfacial term is neglected, i.e., considering the energy of transferring the hydrocarbon tail from hydrocarbon to water, the value $16.6k_{\text{B}}T$ is obtained. This value is also close to the free energy of transferring a dodecane molecule from hydrocarbon to water according to Tanford,[46] $17.2k_{\text{B}}T$.

Other Contributions. The attractive van der Waals force is small, and its contribution to the SDS chemical potential is negligible. Different intermicellar interaction upon varying the adsorption of SDS has also been neglected since only small deviations from $\rho = 1$ are considered.

Computational Procedure. The equilibrium situation is found by requiring the chemical potential of SDS to be equal in the two regions, i.e., in the palisade layer of the micelle and in the aqueous region. The calculation is made in an iterative way as follows:

(1) Choose the bound fraction of SDS, ρ, for one specific sample. This fixes the area per charge and concentration of monomeric SDS (which in the PB calculation is treated as a monovalent salt).

(2) Calculate $\mu^{\text{tot}}_{\text{SDS,mic}}$ and $\mu^{\text{tot}}_{\text{SDS,mon}}$.

(3) Repeat from (1) until $\mu^{\text{tot}}_{\text{SDS,mic}} = \mu^{\text{tot}}_{\text{SDS,mon}}$. At this specific ρ value, the system is in equilibrium.

(4) Continue from (1) with another sample composition.

3.2.3. Comparison with Experiments. The result from the calculation, ρ as function of β and ϕ, is presented in Figure 9. The overall correspondence between experiment and theory is satisfying, noting that no adjustable parameters are used in the calculation. In accordance with experiment, full adsorption (ρ

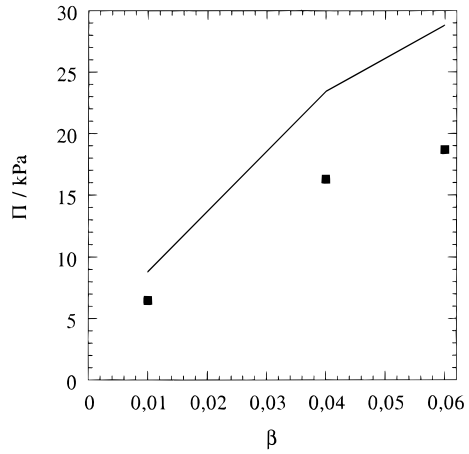

Figure 10. Osmotic pressure as a function of SDS doping, β, at constant concentration, $\phi = 0.34$, in the lamellar phase (■). The lines are the calculated osmotic pressures, assuming full adsorption of SDS into the micellar surfactant film.

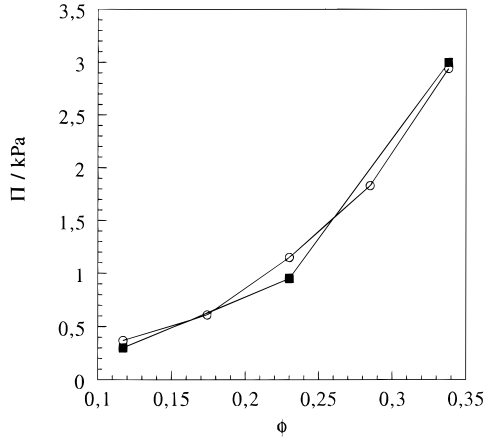

Figure 11. Osmotic pressure versus volume fraction, measured along the lower phase boundary, with $\beta = 0.04$ in 0.1 M NaCl (■). For comparison, the experimental values from the pure microemulsion is also shown (○). The pressures are, within experimental uncertainties, identical. The lines are just guides for the eyes.

$= 1$) is predicted at higher concentrations, $\phi \geq 0.12$. At lower ϕ, $\phi < 0.12$, both theory and experiment gives $0.9 < \rho < 1$. Also in line with the experiments, $\rho(\beta = 0.04) > \rho(\beta = 0.06)$ is predicted.

The $\beta = 0.01$ system, for clarity not shown in the figure, shows a slightly poorer agreement between theory and experiment compared to the $\beta = 0.04$ and $\beta = 0.06$ systems. The reason for the discrepancy in this case presumably originates from ionic impurities. The only electrolyte in the aqueous region that is considered is the nonadsorbed SDS. For $\beta = 0.01$ at $\phi \leq 0.06$, the free SDS concentration is about 2×10^{-5} M, and hence a very small amount of ionic impurities could significantly affect the derived degree of adsorption. This effect is smaller the higher the SDS content, and appears to be negligible in the $\beta = 0.04$ and $\beta = 0.06$ cases. However, remembering that no adjustable parameter is used in the calculation, the correspondence between theoretical and experimental values of ρ is satisfying, indicating that essentially all thermodynamic quantities of relevance are included in our model.

3.2.4. The L_α Phase + SDS. The osmotic pressure was also measured in the lamellar phase at different charge densities. In this case, we fixed the concentration at $\phi = 0.34$, varying only the SDS content, β. The temperatures were 38 °C ($\beta = 0.01$), 44 °C ($\beta = 0.04$), and 52 °C ($\beta = 0.06$). The result is presented in Figure 10. As seen from the figure, Π increases, as expected, monotonically with β. It may be noted that the pressure in the L_α phase is always lower than in the L_1 phase. The full line is the calculated osmotic pressure, assuming full adsorption of SDS ($\rho = 1$). As seen, the calculated curve strongly overestimates the measured pressure. By analyzing this difference, in analogy with the treatment in the L_1 phase, ρ was found to be 0.96, 0.98, and 0.98 for $\beta = 0.01$, 0.04, and 0.06, respectively. These values are somewhat lower than in the L_1 phase, where basically all SDS is located in the micelles at this concentration. The reason for this is not clear.

3.2.5. The L_1 Phase + SDS and NaCl. Exchanging the water with brine (0.1 M NaCl), Π as a function of ϕ in the $\beta = 0.04$ system was measured. The result is presented in Figure 11. The high electrolyte concentration makes the electrostatic contribution to the osmotic pressure negligible, and the droplet interaction resembles the uncharged case. This result confirms that the observed effect of adding small amounts of SDS is purely electrostatic.

Acknowledgment. We are grateful to A.-S. Jönsson and F. Fälth, Chemical Engineering I, Lund University, for their kind assistance during the construction of the osmometer. This work was financially supported by the National Science Research Council (NFR).

References and Notes

(1) Coll, H. *J. Phys. Chem.* **1970**, *74*, 520.
(2) Birdi, K. S. *Kolloid-Z. Z. Polym.* **1972**, *250*, 731.
(3) Birdi, K. S.; Backlund, S.; Soerensen, K.; Krag, T.; Dalsager, S. *J. Colloid Interface Sci.* **1978**, *66*, 118.
(4) Attwood, D.; Elworthy, P. H.; Kayne, S. B. *J. Phys. Chem.* **1970**, *74*, 3529.
(5) Attwood, D.; Elworthy, P. H.; Kayne, S. B. *J. Pharm., Pharmacol.* **1971**, *23*, 77S.
(6) Bagger-Jörgensen, H.; Olsson, U. *Langmuir* **1996**, *12*, 4057.
(7) Parsegian, V. A.; Rand, R. P.; Fuller, N. L. *J. Phys. Chem* **1991**, *95*, 4777.
(8) Zemb, T.; Belloni, L.; Dubois, M.; Marcelja, S. *Prog. Colloid Polym. Sci.* **1992**, *89*, 33.
(9) Olsson, U.; Schurtenberger, P. *Langmuir* **1993**, *9*, 3389.
(10) Bagger-Jörgensen, H.; Olsson, U.; Mortensen, K. *Langmuir* **1997**, *13*, 1413.
(11) Leaver, M. S.; Olsson, U.; Wennerström, H.; Strey, R. *J. Phys. II Fr.* **1994**, 515.
(12) Leaver, M.; Furo′, I.; Olsson, U. *Langmuir* **1995**, *11*, 1524.
(13) Leaver, M. S.; Olsson, U.; Wennerström, H.; Strey, R.; Wurz, U. *J. Chem. Soc., Faraday Trans.* **1994**, *91*, 4269.
(14) Olsson, U.; Würz, U.; Strey, R. *J. Phys. Chem.* **1993**, *97*, 4535.
(15) Rajagopalan, V.; Bagger-Jörgensen, H.; Fukuda, K.; Olsson, U.; Jönsson, B. *Langmuir* **1996**, *12*, 2939.
(16) Leaver, M. S.; Olsson, U. *Langmuir* **1994**, *10*, 3449.
(17) Parsegian, V. A.; Rand, R. P.; Rau, D. C. *Methods Enzymol.* **1986**, *127*, 400.
(18) Flory, P. J. *Polymer Chemistry*, 12th printing ed.; Cornell University Press: Ithaka, NY, 1983.
(19) Platford, R. F. In *Activity Coefficients of Electrolyte Solutions*; Pytkowicz, R. M., Ed.; CRC Press: Boca Raton FL, 1979.
(20) Kauranen, P.; Harwigsson, I.; Jönsson, B. *J. Phys. Chem.* **1994**, *98*, 1411.
(21) Carvell, M.; Hall, D. G.; Lyle, I. G.; Tiddy, G. J. T. *Faraday Discuss. Chem. Soc.* **1986**, *81*, 223.
(22) Aukland, K.; Johnsen, H. M. *Acta Physiol. Scand.* **1974**, *90*, 485.
(23) Dickinson, E.; Goller, M. I.; Wedlock, D. J. *J. Colloid Interface Sci.* **1995**, *172*, 192.
(24) Bonnet-Gonnet, C.; Belloni, L.; Cabane, B. *Langmuir* **1994**, *10*, 4012.
(25) Meguro, K.; Ueno, M.; Esumi, K. In *Nonionic Surfactants: Physical Chemistry*; Schick, M. J., Ed.; Marcel Dekker: New York, 1987; Vol. 23, p 109.
(26) Carnahan, N. F.; Starling, K. E. *J. Chem. Phys.* **1969**, *51*, 635.
(27) Gregory, P.; Huglin, M. B. *Makromol. Chem.* **1986**, *187*, 1745.
(28) Björling, M. *Macromolecules* **1992**, *25*, 3956.
(29) Israelachvili, J. *Intermolecular & Surface Forces*; Academic Press: London, 1991.
(30) Vincent, B. *J. Colloid Interface Sci.* **1973**, *42*, 270.

(31) Mahanty, J.; Ninham, B. W. *Dispersion Forces*; Academic Press: New York, 1976.
(32) Jönsson, A.-S.; Jönsson, B. *J. Colloid Interface Sci.* **1996**, *180*, 504.
(33) Strey, R.; Schomäcker, R.; Roux, D.; Nallet, F.; Olsson, U. *J. Chem. Soc., Faraday Trans.* **1990**, *86*, 2253.
(34) Helfrich, W. *Z. Naturforsch.* **1978**, *33A*, 305.
(35) Helfrich, W. *J. Phys.: Condens. Matter* **1994**, *6*, 79.
(36) Netz, R. R. *Phys. Rev. E* **1995**, *52*, 1897.
(37) Landgren, M.; Aamodt, M.; Jönsson, B. *J. Phys. Chem.* **1992**, *96*, 950.
(38) Kegel, W. K.; Bodnar, I.; Lekkerkerker, H. N. W. *J. Phys. Chem.* **1995**, *99*, 3272.
(39) Fukuda, K.; Olsson, U.; Würz, U. *Langmuir* **1994**, *10*, 3222.
(40) Hill, T. L. *Statistical Mechanics*; Addison and Wesley: Reading, MA, 1960.
(41) Schomäcker, R.; Strey, R. *J. Phys. Chem.* **1994**, *98*, 3908.
(42) Gunnarsson, G.; Jönsson, B.; Wennerström, H. *J. Phys. Chem.* **1980**, *84*, 3114.
(43) Mukerjee, P.; Mysels, K. J. *Crtitical Micelle Concentrations of Aqueous Systems*; NSRDS-NBS 36; U.S. Government Printing Office: Washington, DC, 1971.
(44) Jönsson, B.; Wennerström, H. *J. Colloid Interface Sci.* **1981**, *80*, 482.
(45) Cabane, B.; Duplessix, R.; Zemb, T. *J. Phys. (Paris)* **1985**, *46*, 2161.
(46) Tanford, C. *The Hydrophobic Effect*; Wiley: New York, 1973.